Instability of two-layer film flows due to the interacting effects of surfactants, inertia and gravity

Anna Kalogirou[a)]
School of Mathematics, University of East Anglia, Norwich NR4 7JT, United Kingdom

We consider a two-fluid shear flow where the interface between the two fluids is coated with an insoluble surfactant. An asymptotic model is derived in the thin-layer approximation, consisting of a set of nonlinear PDEs describing the evolution of the film and surfactant disturbances at the interface. The model includes important physical effects such as Marangoni forces (caused by the presence of surfactant), inertial forces arising in the thick fluid layer, as well as gravitational forces. The aim of this study is to investigate the effect of density stratification or gravity – represented through the Bond number Bo – on the flow stability, and the interplay between the different (de)stabilisation mechanisms. It is found that gravity can either stabilise or destabilise the interface (depending on fluid properties), but not always as intuitively anticipated. Different travelling-wave branches are presented for varying Bo and the destabilising mechanism associated with the Marangoni forces is discussed.

Keywords: multilayer flow, surfactants, Marangoni instability, nonlinear dynamical system

I. INTRODUCTION

Multilayer fluid flows are fundamental in a plethora of physical and industrial applications; examples include oxygen flow and transport in lung airways, drug delivery, coating flows, oil recovery, and microfluidics technology[1]. Multilayer flows are, however, mathematically very challenging as they are susceptible to instabilities arising at the interfaces between fluids. They have consequently drawn the attention of many researchers throughout recent decades, with particular emphasis in finding ways to manipulate interfaces and control flows. The ability to control and manipulate multilayer flows is fundamental; one possible approach is by using chemical additives known as surfactants, which can greatly influence such flows especially at small scales.

The effect of surfactants on multilayer flows has been investigated in a variety of different geometries, each one relevant to particular applications; for instance, it was analysed for channel flows[2–5], core-annular flows[6], rod-annular flows[7], and multilayer flows down an inclined plane[8]. The channel flow has received considerably more attention and has served in the literature as an archetype for examining the influence of surfactants on interfacial stability and flow dynamics. The first to study the stability of a clean interface (devoid of surfactants) in channel flows was Yih[9], who found that two-layer Couette-Poiseuille flows can be unstable as long as the Reynolds number is non-zero. Yih's instability is affected by the fluid viscosities, densities and thicknesses, but an essential criterion in its development is a viscosity discontinuity at the interface. It was later found by Hooper[10] that two-layer flows are unstable only when the thinner fluid is more viscous, which since has been known as the

"thin-layer effect". The presence of insoluble surfactant at the interface between the two fluids was shown by Frenkel & Halpern[11,12] to induce linear instability even in the Stokes approximation, and even when there is no viscosity contrast between the fluids.

Since Frenkel and Halpern's discovery, there has been a number of studies investigating the problem further: Blyth & Pozrikidis[3,13] analysed the destabilising effect of inertia and performed numerical simulations in short domains, Frenkel & Halpern[14] solved the problem under the assumption of both layers being thin, while Bassom et al.[4] presented a local model valid in the case where one of the fluid layers is much thinner than the other. The work of Bassom et al.[4] was extended by Kalogirou et al.[15] and Kalogirou & Papageorgiou[5], who solved the full nonlocal system and also examined the effect of inertia on nonlinear saturated solutions. In the latter study, the authors also examined the three-dimensional problem and found that the flow can become unstable to spanwise perturbations (but proved that when inertia is absent, a Squire's type theorem is valid).

A common assumption in the aforementioned studies was that the densities of the two fluids were considered equal, so as to eliminate the effect of gravity and to concentrate on the influence of surfactant on the flow stability. Recently, Frenkel & Halpern[16] extended their previous work[12,14] to add the effect of density stratification and found that for certain parametric ranges, even arbitrarily strong gravitational forces cannot stabilise the flow completely. In this study, we will perform a similar extension to the work presented in Kalogirou & Papageorgiou[5], aiming to investigate the interacting effects of surfactants, gravity and inertia. This paper therefore presents a study that utilises mathematical modelling and numerical computations to scrutinise the influence of density stratification on the stability of surfactant-laden multilayer thin-film shear flows. Understanding stability is essential for efficient flow control in

---

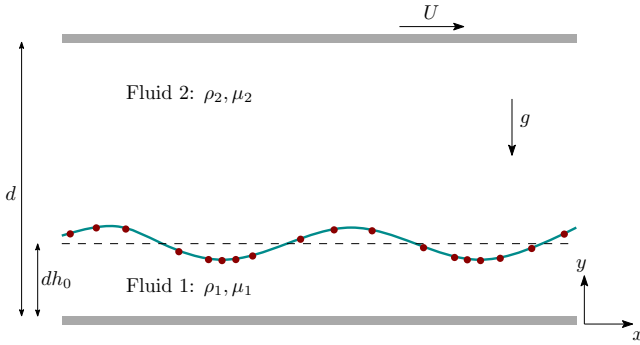[a)]Electronic mail: anna.kalogirou@uea.ac.uk

FIG. 1. Geometry of the problem: two superposed fluid layers in a channel of height d, driven by the upper wall motion with speed U and/or by applying a constant pressure gradient $G = -\frac{\partial p}{\partial x}$. The interface between the two fluids is coated with an insoluble surfactant.

applications where (stable) uniform films or (unstable) interfacial waves are desired. Under the thin-layer approximation, a weakly nonlinear model will be derived for the spatiotemporal evolution of the interfacial and surfactant concentration disturbances. The derived model equation for the film thickness features fundamental components, such as dissipation caused by surface tension, diffusion due to gravity and a nonlocal term due to multiphase coupling. Interfacial instabilities are induced due to the acting forces of gravity and inertia, the existence of a viscosity jump at the interface, as well as the action of Marangoni forces generated as a result of the dependence of surface tension on the local surfactant concentration. Here we will focus mostly on the impact of gravity on linear stability and nonlinear solutions, including saturated travelling waves, their amplitudes and speeds. The underlying physical mechanism responsible for the formation of interfacial waves will also be discussed.

II. MATHEMATICAL MODEL

The problem studied is portrayed in Fig. 1 and described below: two infinitely-long impermeable plates are placed horizontally, parallel to each other and are separated by a distance d. The setup therefore outlines a long horizontal channel defined in two dimensions, with horizontal and vertical coordinates (x, y). The interior of the channel is occupied by two superposed layers of viscous and immiscible fluids, separated by a distinct interface at $y = dh_0$, with $0 < h_0 < 1$. The two fluids are denoted as fluid 1 and 2 (bottom and top fluid, respectively) and have in general different thicknesses, densities ρ_1, ρ_2 and viscosities μ_1, μ_2. We consider the flow driven by the motion of the upper channel wall with speed U (both walls could be allowed to move, but here we consider the lower wall to be stationary), or by combination of upper wall motion and a constant pressure gradient $G = -\frac{\partial p}{\partial x}$.

The action of different forces such as gravity and iner-

tia can be responsible for the generation of instabilities at the interface between the fluids[17,18], in which case the interface is deformed to a general shape $y = h(x, t)$. In this study we are interested in a scenario where the interface is also coated with an insoluble surfactant, which is only allowed to move on the interface and whose local concentration is denoted by $\Gamma(x, t)$. The presence of surfactant affects the interfacial surface tension by lowering its value and therefore it is anticipated to make the interface more susceptible to instabilities, due to the generation of the so-called Marangoni forces. Here we consider dilute surfactant concentrations only and therefore a linear equation of state is expected to be valid. The surface tension γ is reduced according to the local surfactant concentration Γ, following a linearised Langmuir isotherm by

$$\gamma = \gamma_c \left(1 - \beta \frac{\Gamma}{\Gamma_\infty}\right), \quad (1)$$

where γ_c is the surface tension of a clean interface in the absence of surfactants, β is a parameter that measures the sensitivity of interfacial tension to changes in the surfactant concentration[19], and Γ_∞ is the surfactant concentration at maximum packing.

In order to express the problem in non-dimensional form, the channel height d is used to scale lengths, the upper wall speed U to scale velocities, fluid pressures are scaled by $\rho_1 U^2$, time by $\frac{d}{U}$, surface tension is scaled by γ_c and surfactant concentration by Γ_∞. A number of dimensionless parameters are therefore introduced: the density and viscosity ratios

$$r = \frac{\rho_2}{\rho_1}, \quad m = \frac{\mu_2}{\mu_1}, \quad (2)$$

(we also define $r_i = \rho_i/\rho_1$ and $m_i = \mu_i/\mu_1$, $i = 1, 2$, such that $r_1 = 1$, $r_2 = r$ and $m_1 = 1$ and $m_2 = m$), the *Reynolds* number in each fluid,

$$Re_1 = \frac{\rho_1 U d}{\mu_1}, \quad Re_2 = \frac{\rho_2 U d}{\mu_2} = \frac{r}{m} Re_1, \quad (3)$$

and the *Froude*, *Bond*, *Weber*, *Capillary*, *Marangoni* and *Peclét* numbers, defined by

$$Fr = \frac{U}{\sqrt{gd}}, \quad Bo = \frac{(1-r)d^2\rho_1 g}{\gamma_c}, \quad We = \frac{\rho_1 U^2 d}{\gamma_c},$$
$$Ca = \frac{\mu_1 U}{\gamma_c}, \quad Ma = \frac{\beta}{Ca}, \quad Pe = \frac{Ud}{\mathcal{D}_s}, \quad (4)$$

respectively. Here, g denotes the gravitational acceleration and $\mathcal{D}_s$ the diffusivity of surfactant along the interface.

The flow in each fluid region $i = 1, 2$ is described by the non-dimensional Navier-Stokes equations and the continuity equation, given by

$$\frac{\partial \boldsymbol{u}_i}{\partial t} + \boldsymbol{u}_i \cdot \nabla \boldsymbol{u}_i = -\frac{1}{r_i}\nabla p_i + \frac{1}{Re_i}\nabla^2 \boldsymbol{u}_i + \boldsymbol{F}, \quad (5a)$$
$$\nabla \cdot \boldsymbol{u}_i = 0, \quad (5b)$$

where $\boldsymbol{u}_i(x,y,t) = (u_i, v_i)$, $i = 1, 2$, denotes the velocity in each region and $p_i(x,y,t)$, $i = 1, 2$, the pressure. Here, $\nabla = (\frac{\partial}{\partial x}, \frac{\partial}{\partial y})$ and the body force vector is defined by $\boldsymbol{F} = (0, -\frac{1}{Fr^2})$.

The boundary and interfacial conditions associated with the problem are the following: no-slip and no-penetration conditions are imposed on the two walls, i.e. $\boldsymbol{u}_1 = (0,0)$ at $y = 0$ and $\boldsymbol{u}_2 = (1,0)$ at $y = 1$, while at the interface $y = h(x,t)$ velocity continuity $\boldsymbol{u}_1 = \boldsymbol{u}_2$ must be satisfied, together with a kinematic condition

$$v_1 = h_t + u_1 h_x, \tag{6}$$

and continuity of normal and tangential stresses

$$\left[-p_i\left(1 + h_x^2\right) + \frac{2r_i}{Re_i}\left(h_x^2 u_{ix} + v_{iy} - h_x\left(u_{iy} + v_{ix}\right)\right) \right]_2^1$$
$$= \frac{(1 - \beta\Gamma)}{We}\frac{h_{xx}}{\sqrt{1 + h_x^2}}, \tag{7a}$$

$$\left[2m_i h_x\left(u_{ix} - v_{iy}\right) + m_i\left(h_x^2 - 1\right)\left(u_{iy} + v_{ix}\right) \right]_2^1$$
$$= Ma\,\Gamma_x\sqrt{1 + h_x^2}, \tag{7b}$$

with $[f_i]_2^1 = f_1 - f_2$ denoting the jump across the interface. The terms on the right-hand-side in both the normal and tangential stress balance indicate the dependence of the surface tension on the local surfactant concentration. The surface-tension gradients in the tangential stress balance (7b) in particular, emerge due to local changes in the surfactant concentration and give rise to Marangoni forces.

Finally, variations in the interfacial surfactant concentration due to surface convection and molecular diffusion along the deformed interface are described by a dimensionless conservation equation of the form

$$\Gamma_t + \frac{h_x h_{tx}}{1 + h_x^2}\Gamma + \frac{1}{\sqrt{1 + h_x^2}}\left(\sqrt{1 + h_x^2}\,u_1(h)\Gamma\right)_x$$
$$= \frac{1}{Pe}\frac{1}{\sqrt{1 + h_x^2}}\left(\frac{\Gamma_x}{\sqrt{1 + h_x^2}}\right)_x. \tag{8}$$

A. Basic steady flow

In the unperturbed and surfactant-free state, the interface between the fluids is planar and the momentum equations (5a) admit a steady unidirectional flow (a Couette-Poiseuille flow). The exact steady solution can be obtained by solving the momentum equations in both fluids, applying the boundary conditions and interfacial velocity continuity, and satisfying continuity of pressure (7a) and shear stress (7b) at the interface. The basic flow in each fluid layer $i = 1, 2$ is hence found to be

$$\bar{u}_i = -\frac{1}{2}A_i y^2 + B_i y + C_i, \quad \bar{v}_i = 0, \tag{9a}$$

$$\bar{p}_i = P_0 - \frac{r_i}{Fr^2}(y - h_0) - Kx, \tag{9b}$$

where P_0 is the undisturbed constant pressure at the interface and the coefficients A_i, B_i, C_i are given by

$$A_2 = \frac{1}{m}Re_1 K, \quad B_2 = \frac{1 + \frac{1}{2}A_2\left(1 + h_0^2(m - 1)\right)}{1 + h_0(m - 1)}, \tag{9c}$$

$$C_2 = (m - 1)h_0\left(\frac{1 + \frac{1}{2}A_2(1 - h_0)}{1 + h_0(m - 1)}\right), \tag{9d}$$

and $A_1 = mA_2$, $B_1 = mB_2$, $C_1 = 0$. The non-dimensional pressure gradient $K = -\frac{\partial\bar{p}_i}{\partial x} > 0$ is a constant; it is connected to the dimensional constant G through $G = \frac{\rho_1 U^2}{d}K$. The above solution is identical to the one found in Bassom et al.[4] if we set gravity to zero, i.e. take $Fr^{-1} = 0$.

B. Asymptotic approximation for thin lower layers

In what follows, the lower layer is assumed to be very thin in comparison to the upper layer, i.e. we set $h_0 = \epsilon$, with $\epsilon \ll 1$. The typical approach followed when one length scale (here the interface height) is much smaller than the others (here the channel height and length) is the lubrication approximation. The lubrication approximation was used by Halpern & Frenkel[2] to build a model valid for interfacial deformations of the same order as the film thickness. In this work, the objective is to derive a nonlinear evolution equation for the film thickness that also depends on the perturbations in the overlying thick fluid. We note that coupling between the two fluid layers is not possible when the usual lubrication theory is applied, as the interfacial perturbation does not induce a sufficiently large disturbance in the thick fluid. Following a weakly nonlinear analysis, however, allows for the coupling between the two fluids to remain in the leading-order dynamics as will be seen next. We therefore introduce a small perturbation to the interface and local surfactant concentration by

$$h(x,t) = \epsilon + \epsilon^2 H(x,t), \qquad \Gamma(x,t) = \delta\tilde{\Gamma}(x,t), \tag{10}$$

with $H, \tilde{\Gamma} = \mathcal{O}(1)$ and $\delta = \delta(\epsilon) \ll 1$. Order-one rescaling parameters Ca_0, Ma_0, Pe_0 are also introduced by[6] $Ca = \epsilon Ca_0$, $Ma = \epsilon^2\delta^{-1}Ma_0$, $Pe = \epsilon^{-2}Pe_0$, while the rest of the parameters such as the density ratio r, viscosity ratio m and Reynolds numbers Re_1, Re_2 are assumed to be $\mathcal{O}(1)$. The above parameter rescalings are required in order to keep important features such as surface tension damping, Marangoni stresses and surfactant diffusivity in the final evolution equations. When the interface in perturbed according to (10), a velocity and pressure jump appear at the interface; these can be found by evaluating (9) at $h = \epsilon + \epsilon^2 H$ and are given by

$$\bar{u}_1 - \bar{u}_2\big|_{y=h} = (m - 1)\left(1 + \frac{A_2}{2}\right)\epsilon^2 H, \tag{11a}$$

$$\bar{p}_1 - \bar{p}_2\big|_{y=h} = \frac{(r - 1)}{Fr^2}(h - \epsilon) = -\frac{Bo}{Ca_0 Re_1}\epsilon H, \tag{11b}$$

where we have used the relations $\frac{(1-r)}{Fr^2} = \frac{Bo}{We}$ and $We = CaRe_1 = \epsilon Ca_0 Re_1$. Notice that the pressure jump across the interface only arises when the densities of the fluids are different, *i.e.* for $Bo \neq 0$.

The subsequent analysis follows closely on derivations presented previously[4–6,15], although this work is distinguished from earlier studies by considering the more general problem with fluids of different densities. The main steps of the derivation of the model equations are outlined below. In fluid 1, a new order-one vertical coordinate is introduced by $\xi = y/\epsilon$ and the flow expands as follows

$$
\begin{aligned}
u_1 &= \bar{u}_1(\xi; \epsilon) + \epsilon^3 \tilde{u}_1(x, \xi, t) + \cdots, \\
v_1 &= \epsilon^4 \tilde{v}_1(x, \xi, t) + \cdots, \\
p_1 &= \bar{p}_1(x, \xi) + \epsilon \tilde{p}_1(x, \xi, t) + \cdots,
\end{aligned}
\tag{12a}
$$

while in fluid 2 the flow is perturbed away from the basic state by

$$
\begin{aligned}
u_2 &= \bar{u}_2(y) + \epsilon^2 \tilde{u}_2(x, y, t) + \cdots, \\
v_2 &= \epsilon^2 \tilde{v}_2(x, y, t) + \cdots, \\
p_2 &= \bar{p}_2(x, y) + \epsilon^2 \tilde{p}_2(x, y, t) + \cdots,
\end{aligned}
\tag{12b}
$$

with perturbation variables $\tilde{u}_1, \tilde{v}_1, \tilde{p}_1, \tilde{u}_2, \tilde{v}_2, \tilde{p}_2 = \mathcal{O}(1)$. Substituting expansions (12a) in the non-dimensional Navier-Stokes equations (5) and working with leading-order perturbation terms only, results in the standard lubrication equations[2,4,14], given by

$$
0 = -\frac{\partial \tilde{p}_1}{\partial x} + \frac{1}{Re_1}\frac{\partial^2 \tilde{u}_1}{\partial \xi^2}, \tag{13a}
$$

$$
0 = -\frac{\partial \tilde{p}_1}{\partial \xi}, \tag{13b}
$$

$$
\frac{\partial \tilde{u}_1}{\partial x} + \frac{\partial \tilde{v}_1}{\partial \xi} = 0. \tag{13c}
$$

The same expansions are also inserted into the normal stress balance (7a), yielding at leading order

$$
\tilde{p}_1 = -\frac{1}{Re_1 Ca_0}(H_{xx} - BoH), \tag{14}
$$

where the basic pressure jump across the interface (11b) has been used. Similarly, the tangential stress balance (7b) at leading order becomes

$$
-\frac{\partial \tilde{u}_1}{\partial \xi}\bigg|_{\xi=1} + m\left(\frac{\partial \tilde{u}_2}{\partial y} + \frac{\partial \tilde{v}_2}{\partial x}\right)\bigg|_{y=0} = Ma_0 \frac{\partial \Gamma}{\partial x}. \tag{15}
$$

Equation (13b) yields that $\tilde{p}_1$ is independent of the vertical coordinate ξ, hence the pressure perturbation at the interface (14) is valid everywhere in the film. Equation (14) is inserted into (13a), which is then integrated across the film twice (the constants of integration are specified by using condition (15) at $\xi = 1$ and the no-slip condition at $\xi = 0$) to give the horizontal velocity perturbation in the film $\tilde{u}_1$. That is substituted into the continuity equation (13c), which – after one more integration – yields the vertical velocity perturbation in the film $\tilde{v}_1$. The obtained horizontal and vertical velocity perturbations in the film $\tilde{u}_1, \tilde{v}_1$ are required in the kinematic condition at the interface $\xi = 1$.

The kinematic equation (6) is then considered and perturbations (10)-(12) are applied. A Galilean transformation to a frame of reference moving with the undisturbed interfacial velocity and a slow-time scale are introduced by

$$
\tilde{x} = x - \bar{u}_1(\epsilon)t, \qquad \tilde{t} = \epsilon^2 t. \tag{16}
$$

This step is performed in order to remove a linear term and to allow other essential terms to remain in the leading-order equation, namely time-dependence, non-linearity and dissipation. The leading-order kinematic condition hence converts into

$$
H_{\tilde{t}} + \left(m + \frac{A_1}{2}\right)HH_{\tilde{x}} + \frac{1}{3Ca_0}(H_{\tilde{x}\tilde{x}\tilde{x}\tilde{x}} - BoH_{\tilde{x}\tilde{x}})
$$
$$
+ \frac{m}{2}T\big|_{y=0} - \frac{Ma_0}{2}\tilde{\Gamma}_{\tilde{x}\tilde{x}} = 0, \tag{17}
$$

where $T(\tilde{x}, y) = \tilde{u}_{2\tilde{x}y} + \tilde{v}_{2\tilde{x}\tilde{x}}$ originates from the tangential stress balance (7b) (or (15)) and is constructed by solving the problem in the upper fluid layer; it provides coupling between lower and upper layers and is the source of non-locality in the final evolution system. The term $T(\tilde{x}, y)$ is required at the interface $y = \epsilon + \epsilon^2 H \approx 0$ and is found to be (the hat denotes a Fourier transform)

$$
T\big|_{y=0} = \frac{i}{\pi}(1-m)\left(1 + \frac{A_2}{2}\right)\int_{-\infty}^{+\infty} \mathcal{N}(k)\hat{H}(k)e^{ik\tilde{x}}\,\mathrm{d}k, \tag{18}
$$

where $\mathcal{N}(k) = -\frac{k}{2}F''(0)$ and $F(y)$ is the solution of an Orr-Sommerfeld type problem in the thick fluid layer[4,5] – more details are provided in Appendix A. Note that the dynamics in the upper layer are governed by the effects of inertia, represented by the Reynolds number Re_2 which appears in the Orr-Sommerfeld problem and therefore affects the solution of $F(y)$ and $\mathcal{N}(k)$ (from now on, the subscript from Re_2 will be omitted and R_e will be used instead).

What is left is to consider the surfactant convection-diffusion equation (8) and analyse how this is transformed under perturbations (10), asymptotic expansions (12) and transformations (16). At leading order the equation becomes

$$
\tilde{\Gamma}_{\tilde{t}} + \left(m + \frac{A_1}{2}\right)\left(H\tilde{\Gamma}\right)_{\tilde{x}} = \frac{1}{Pe_0}\tilde{\Gamma}_{\tilde{x}\tilde{x}}. \tag{19}
$$

C. Final evolution equations

The derivation of the mathematical model is complete, but as a last step the tildes are dropped and the following

canonical rescaling is applied

$$H \rightarrow \left(3Ca_0\left(m + \frac{A_1}{2}\right)\right)^{-1} H, \qquad t \rightarrow 3Ca_0\, t,$$

$$\Gamma \rightarrow 2\left(\left(m + \frac{A_1}{2}\right)(3Ca_0)^2 Ma_0\right)^{-1} \Gamma. \qquad (20)$$

The final evolution equations for the perturbations of the film thickness and local surfactant concentration are given by

$$H_t + HH_x - BoH_{xx} + H_{xxxx}$$
$$+ \frac{i\Lambda}{2\pi}\int_{-\infty}^{+\infty} \mathcal{N}(k)\hat{H}(k)\mathrm{e}^{ikx}\,\mathrm{d}k - \Gamma_{xx} = 0, \qquad (21a)$$

$$\Gamma_t + (H\Gamma)_x - \eta\Gamma_{xx} = 0. \qquad (21b)$$

Two new parameters are introduced in the above system, defined by

$$\Lambda = 3\,Ca_0\, m(1-m)\left(1 + \frac{A_2}{2}\right), \quad \eta = \frac{3Ca_0}{Pe_0}. \qquad (22)$$

Parameter Λ is mainly used to express the effect of viscosity stratification (but it also depends on the Poiseuille-flow pressure gradient A_2); it is positive if $m < 1$, $i.e.$ when the film is more viscous than the upper layer fluid, and negative otherwise. The second parameter η controls the amount of surfactant surface diffusivity.

The reduced system of evolution equations (21) is derived under the assumption of small perturbations to the thickness of a thin film, but nevertheless it retains a number of salient physical properties listed next:

- Both equations are nonlinear and coupled in H and Γ, which allows for saturation of linear waves to nonlinear structures – mostly pulse-like travelling waves of long wavelength, as will be seen later.
- Marangoni forces come into play through the Γ_{xx} term in the film thickness evolution equation.
- Gravitational forces are incorporated in the diffusion term $-BoH_{xx}$ and are responsible for making the flow susceptible to the classical Rayleigh-Taylor instability[20] that appears when a heavy fluid lies above a lighter fluid. This scenario emerges only when the Bond number coefficient is negative, $i.e.$ if $r > 1$, in which case the diffusion term destabilises the problem. The corresponding term causes stabilisation of the interface when the fluids are stably stratified ($r < 1$).
- Damping of short waves is induced through the H_{xxxx} term and is caused by surface-tension forces[21].
- Inertial effects in the thick fluid layer are included in the nonlocal integral term[4,5], which depends on the Reynolds number of the thick fluid R_e.

We note that the thin-film model (21) is also valid for a flow in an inclined channel. The only change in that situation would be in the parameter A_2 that comes from the basic flow (see (9c)), which appears in the definition

of Λ in (22) and in the solution of $\mathcal{N}(k)$. In a horizontal channel, A_2 is non-zero only in the presence of pressure gradient, but if the channel is inclined then A_2 becomes $A_2 = \frac{1}{m}Re_1\left(K + \frac{r}{Fr^2}\sin\theta\right)$, with θ the angle of inclination. Therefore this modification does not introduce any new parameters in the problem but only affects the amount of inertia in the problem.

III. LINEAR STABILITY THEORY

The problem considered is satisfied by a uniform solution $H = 0$ and $\Gamma = \Gamma_0 = $ constant. To investigate the linear stability properties of the system, normal-mode perturbations are introduced by $H(x,t) = \delta\mathrm{e}^{\sigma t + ikx}\tilde{H}$, $\Gamma(x,t) = \Gamma_0 + \delta\mathrm{e}^{\sigma t + ikx}\tilde{\Gamma}$, with complex growth rate σ, real wavenumber k and eigenvectors $\tilde{H}$, $\tilde{\Gamma}$. Instability of the uniform state is supported when the real part of σ is positive, in which case linear solutions grow exponentially in time. Substituting the normal-mode solutions into equations (21), results in

$$\left(\sigma + Bok^2 + k^4 + i\Lambda\mathcal{N}(k)\right)\tilde{H} + k^2\tilde{\Gamma} = 0, \qquad (23a)$$

$$\left(\sigma + \eta k^2\right)\tilde{\Gamma} + ik\Gamma_0\tilde{H} = 0. \qquad (23b)$$

The above linear system can be written in a matrix form as $M\boldsymbol{x} = 0$, with coefficient matrix M and vector of unknowns $\boldsymbol{x} = (\tilde{H}, \tilde{\Gamma})^T$. A nontrivial solution $\boldsymbol{x} \neq \boldsymbol{0}$ is possible when the determinant of the matrix M is zero, in which case a dispersion relation for σ can be obtained.

Stratified flows are known to be susceptible to long-wave instabilities[9–11], so it is sufficient to consider a long-wave approximation of the nonlocal term $\mathcal{N}(k)$ in (23) ($i.e.$ an expansion for small wavenumbers k). The resulting dispersion relation for long waves is given by

$$\sigma^2 + \left[2i\Lambda k + Bok^2 - \frac{\Lambda R_e}{60}\left(1 + \frac{A_2}{14}\right)k^2 + \eta k^2\right]\sigma$$
$$+ (2\eta\Lambda - \Gamma_0)ik^3 = 0. \qquad (24)$$

This is a second-order polynomial in σ consequently there are two modes $\sigma_{1,2}$, one interfacial and one surfactant mode. The flow is unstable to long wavelength perturbations if at least one of the two modes has a positive real part. The two amplification rates $s_{1,2} = \Re(\sigma_{1,2})$ are found to be (assuming $\Lambda \neq 0$)

$$s_1 = \frac{(\Gamma_0 - 2\eta\Lambda)}{2\Lambda}k^2,$$

$$s_2 = \left[\frac{\Lambda R_e}{60}\left(1 + \frac{A_2}{14}\right) - \frac{\Gamma_0}{2\Lambda} - Bo\right]k^2, \quad k \ll 1. \qquad (25)$$

In the absence of density stratification, that is $r = 1$ and $Bo = 0$, the above expressions are identical to the ones presented in Bassom et al.[4] and Kalogirou & Papageorgiou[5] (for their $k_1 = k$ and $k_2 = 0$).

Typical unstable growth rates are demonstrated in Fig. 2 for different values of η in $[0,1]$ (some growth rates
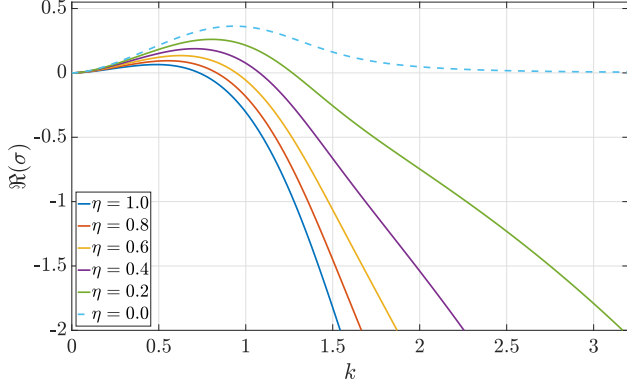
FIG. 2. Effect of decreasing η on unstable growth rates. The parameter values used are: $R_e = 25$, $\Lambda = 0.25$, $Bo = 0$, $A_2 = 0$, $\Gamma_0 = 1$, and $\eta = 1.0, 0.8, 0.6, 0.4, 0.2, 0.0$ (dashed line).

are also shown in Fig. 4 in the next section). For $\eta \neq 0$, the unstable growth rates get stabilised below a critical value of the wavenumber k, a common behaviour of dissipative systems (the short-wave stabilisation is due to surface tension). The two growth rates for large wavenumbers are $\sigma_1 = -\eta k^2$, $\sigma_2 = -k^4$, which can be obtained by finding the dispersion relation in the large-k limit. The first growth rate $\sigma_1 \to 0$ when $\eta \to 0$ as illustrated by the dashed line in Fig. 2 (whereas σ_2 remains unaffected), in which case the problem is ill-posed; physically, this corresponds to no diffusion of surfactant at the interface. On the contrary, the model presented in Frenkel & Halpern[14], which does not include surfactant diffusion at the interface but only interfacial convection, is shown to be well-behaved in the zero-diffusion limit. We believe this discrepancy to be due to the thin-film assumption, considering that both Frenkel & Halpern[14] and Blyth & Pozrikidis[3] solved the problem for comparable fluid thicknesses and found the zero-diffusion limit to be continuous.

The surfactant-free problem can be obtained by taking the limit $\eta \to \infty$; this physically corresponds to infinitely large surfactant diffusivity, which is associated with a uniform surfactant distribution along the interface[3]. Setting $\eta \to \infty$ in (23b) yields $\tilde{\Gamma} = 0$, thereby providing a linear dispersion relation for the interfacial mode given by the coefficient of $\tilde{H}$ in (23a). The condition for instability is provided by the second growth rate s_2 in (25) with $\Gamma_0 = 0$ (the growth rate s_1 is now irrelevant), corresponding to a clean interface with uniform surface tension. The surfactant-free interface is unstable to long waves when s_2 is positive, which can happen in one of the following scenarios (we assume $R_e > 0$ and $A_2 \geq 0$):

1. $\Lambda \leq 0$ and $Bo < \frac{\Lambda R_e}{60}\left(1 + \frac{A_2}{14}\right) \leq 0$, corresponding to a heavier overlying fluid (destabilisation due to density stratification);

2. $Bo \geq 0$ and and $0 \leq Bo < \frac{\Lambda R_e}{60}\left(1 + \frac{A_2}{14}\right)$, corresponding to a more viscous thin film (destabilisa-

tion due to viscosity stratification);

3. $\Lambda > 0$ and $Bo < 0$ (destabilisation due to both density and viscosity stratification).

These remarks are in line with the results of Yih[9] in the limit of thin lower layer ($n \to 0$ in Yih's notation).

The growth rates in (25) are also useful in determining the neutral stability curves, given by

$$\Gamma_0 - 2\eta\Lambda = 0,$$

$$\Lambda^2 R_e\left(1 + \frac{A_2}{14}\right) - 30\Gamma_0 - 60\Lambda Bo = 0, \quad (26)$$

which can be then plotted to produce a linear stability diagram in parameter space. We choose to fix parameters Bo, A_2, Γ_0, η and present the stability diagram in the $\Lambda - R_e$ parameter space. The stability diagram demonstrating the neutral-stability curves (solid lines), together with regions of stability and instability in the $\Lambda - R_e$ space, is provided in Fig. 3. The instability region for equal-density fluids is shaded with a grey colour (the linear stability diagram in this case is identical to Fig. 2 in Kalogirou & Papageorgiou[5]), while the effect of density stratification is shown with pink-shaded regions, for $Bo > 0$ in panel (a) and $Bo < 0$ in panel (b). The critical points Λ_c and $R_{e,c}$ define the location where the neutral curves cross each other and are given by

$$\Lambda_c = \frac{\Gamma_0}{2\eta}, \qquad R_{e,c}\left(1 + \frac{A_2}{14}\right) = \frac{120\eta}{\Gamma_0}\left(\eta + Bo\right). \quad (27)$$

An interesting feature seen in both panels of Fig. 3 is that the neutral curves can now pass through the Λ-axis and the flow can become stable below a cut-off value of Λ; this is true for any non-zero value of the Bond number $Bo \neq 0$. The critical value of Λ can be obtained by setting $R_e = 0$ in (26) and is found to be $\Lambda_* = -\frac{\Gamma_0}{2Bo}$. If $Bo > 0$ and the fluids are stably stratified, the flow becomes stable beyond a critical point $\Lambda_* < 0$ (Fig. 3(a)) and at the same time the region of instability shrinks (pink area is smaller than grey area). On the other hand if $Bo < 0$ and the overlying fluid is more heavy, the flow becomes unstable beyond $\Lambda_* > 0$. The implication of the latter is the complete disappearance of the (white) stability region seen in the $\Lambda > 0$ quadrant when $Bo \leq -\eta < 0$ (note that when $Bo = -\eta$, then $\Lambda_c = \Lambda_*$ and $R_{e,c} = 0$ – this is the case shown in Fig. 3(b)). The (de)stabilisation beyond a critical point Λ_* has not been observed for equal-density fluids[5], in which case the neutral curves approach the Λ-axis asymptotically and consequently unstable waves (of some wavelength) can always be found.

While the flow destabilisation in the case where a heavy fluid lies above a lighter fluid is physically anticipated (even though Charru & Fabre[22] reported a shear-stress stabilisation of analogous flows), a counterintuitive result can be seen in Fig. 3(a). That is, the unstable region between $0 < \Lambda < \Lambda_c$ remains unaffected despite how strong the stabilising influence of gravity is (note that Fig. 3(a) uses $Bo > 0$ and gravity has a stabilising effect because the lower fluid is the heavier). A similar
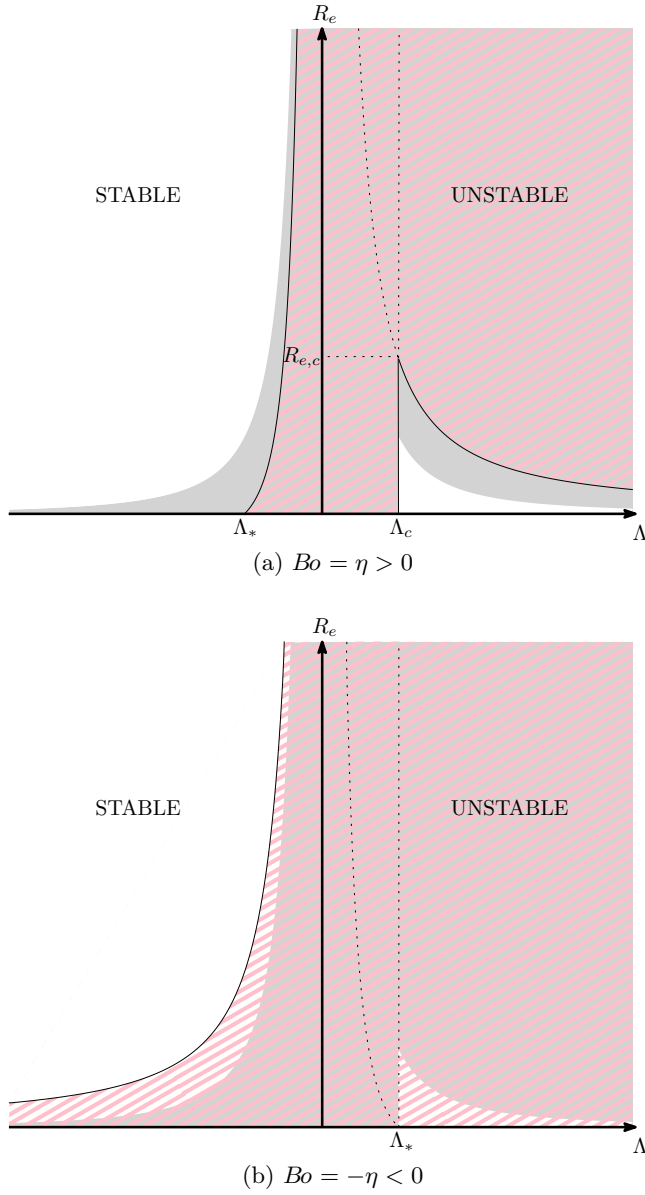
(a) $Bo = \eta > 0$

(b) $Bo = -\eta < 0$

FIG. 3. Effect of the Bond number on the linear stability diagram of Kalogirou & Papageorgiou[5] (adapted with permission from *J. Fluid Mech.* **802**, 2016). Regions of instability are denoted with grey colour for $Bo = 0$ and pink colour for $Bo \neq 0$. The top panel presents a case with stably stratified fluids and $Bo > 0$, while in the bottom panel $Bo < 0$ and the stratification is unstable.

result has also been observed by Frenkel & Halpern[16] and shows that the Marangoni forces generated at the interface due to the presence of surfactants are strong enough to overcome the effect of gravity, whose role is expected to be comparatively weak in small scales.

IV. NUMERICAL COMPUTATIONS

A. Governing equations on periodic domains

The system (21) describing the evolution of the flow is solved numerically on finite L-periodic domains, in which case the nonlocal term has a Fourier series representation. For convenience we first rescale the evolution equations onto the canonical domain $[0, 2\pi]$ using the transformations $x \to (L/2\pi)x$, $t \to (L/2\pi)^2 t$, $H \to (2\pi/L)H$, $\Gamma \to (2\pi/L)\Gamma$, and seek solutions to the initial-value problem

$$H_t + HH_x - BoH_{xx} + \nu H_{xxxx}$$

$$+ i\Lambda\nu^{-1} \sum_{k=-\infty}^{+\infty} \mathcal{N}(k\sqrt{\nu})\,\hat{H}(k)\,e^{ikx} - \Gamma_{xx} = 0, \quad (28a)$$

$$\Gamma_t + (H\Gamma)_x - \eta\Gamma_{xx} = 0, \quad (28b)$$

$$H(x,0) = \alpha\nu^{-1/2}\sin(nx), \quad \Gamma(x,0) = \Gamma_0\nu^{-1/2}, \quad (28c)$$

where $\hat{H}(k)$ denotes the Fourier coefficients of $H(x,t)$, α is the initial amplitude (chosen between 10^{-3} and 10^{-1} in the computations), and n is the wavelength of the initial perturbation. An important new bifurcation parameter ν also appears in the above system, defined by $\nu = (2\pi/L)^2$. Reducing the value of ν corresponds to increasing the length L and this results in more unstable modes entering into the dynamics – a detailed study on the role of ν in the generation of complex spatiotemporal dynamics for $Bo = 0$ can be found in Kalogirou & Papageorgiou[5].

The spatial periodicity of the problem allows the use of spectral methods. The set of equations (28) are transformed in Fourier space, where a pseudospectral representation of spatial derivatives can be applied and the nonlocal term in (28a) is known exactly. The time discretisation of the system is performed by use of implicit-explicit BDF schemes[23] (with an implicit discretisation of the linear part of the system and an explicit discretisation of the nonlinear part). Such methods are presented and analysed in detail in Akrivis et al.[24] and Akrivis & Smyrlis[25], hence we refer the reader to those studies for more details on the implementation of the schemes.

B. Validation of linear theory

We start our numerical investigation by comparing the numerically obtained solutions to the expectations of linear theory. We thus perform nonlinear computations with a small-amplitude initial condition $\alpha = 10^{-3}$ and short final time $t = 10$; this ensures that the solutions obtained are still in the linear regime and have not yet saturated to a nonlinear state. The initial perturbation has a wavelength equal to the domain length (*i.e.* we choose $n = 1$) and select the remaining parameters such
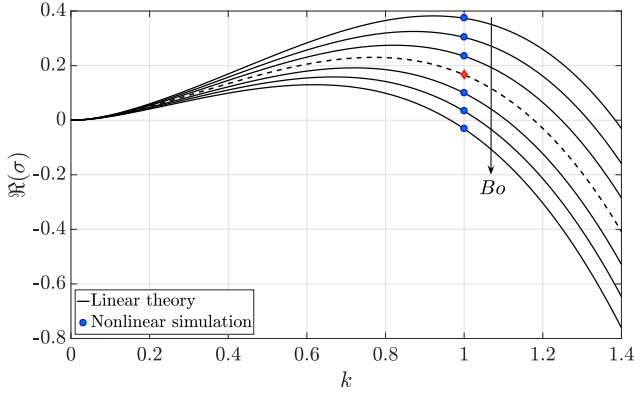
FIG. 4. Effect of the Bond number on unstable growth rates. The blue circles depict the growth-rate prediction from the nonlinear simulation. The parameter values used are: $\nu = 0.4$, $R_e = 25$, $\Lambda = -0.25$, $A_2 = 0$, $\Gamma_0 = 1$, $\eta = 1$, and $Bo = -0.3, -0.2, -0.1, 0.0, 0.1, 0.2, 0.3$. The arrow indicates the direction of increasing Bond number. The dashed line and red diamond correspond to the theoretical and numerical growth rates for $Bo = 0$.

that only the first mode is unstable and the rest of the modes are dampened.

In the linear regime, the solution $H(x, t)$ takes the form $H = \delta e^{\sigma t + ikx}\tilde{H}$ (a similar statement holds for $\Gamma(x, t)$), therefore the L_2-norm becomes $\|H\| = \delta e^{\sigma t}\|e^{ikx}\tilde{H}\|$. The calculation of the logarithm $\log(\delta^{-1}\|H\|)$ results in a linear function of the form $f(t) = \sigma t + $const. (after some initial transients), whose slope can be approximated using polynomial interpolation (here we use first-order interpolation). The leading-order coefficient of the interpolated polynomial then provides the linear growth-rate prediction from the nonlinear simulation, depicted in Fig. 4 with blue circles for increasing values of the Bond number (the value of the Bond number increases in the direction of the arrow). For reference, the theoretical and numerical growth rates for $Bo = 0$ are also shown with dashed line and red diamond, respectively. Clearly, there is a critical value of the Bond number between 0.2 and 0.3, above which the growth rate at $k = 1$ (corresponding to waves of wavelength 2π) becomes negative and the waves are stabilised. The exact critical value of the Bond number corresponding to the set of parameters used in Fig. 4 is $Bo_c = 0.2509$, as will be seen in Table I later.

C. Nonlinear results

In this section we present nonlinear saturated structures obtained numerically. Kalogirou & Papageorgiou[5] demonstrated a dynamically complex saturation of the thin-film system, through carrying out extensive numerical computations of the initial-value problem (28) for a range of parameter values that support interfacial instabilities (in the absence of gravity, $Bo = 0$). Our interest

ν	0.4	0.3	0.2	0.2	0.1
Λ	-0.25	-0.25	-0.25	0.25	0.25
Bo_c	0.2509	0.4403	0.6721	0.8558	1.44

TABLE I. Critical values of the Bond number Bo_c for some representative values of ν and Λ, and for fixed $R_e = 25$, $A_2 = 0$, $\Gamma_0 = 1$, $\eta = 1$. Below these cut-off values, long waves become unstable to perturbations of wavelength equal to the domain size. For the set of parameters corresponding to the last column, we have also found the critical value for instability to perturbations of wavelength equal to the half of the domain size; this is given by $Bo_c = 0.3112$.
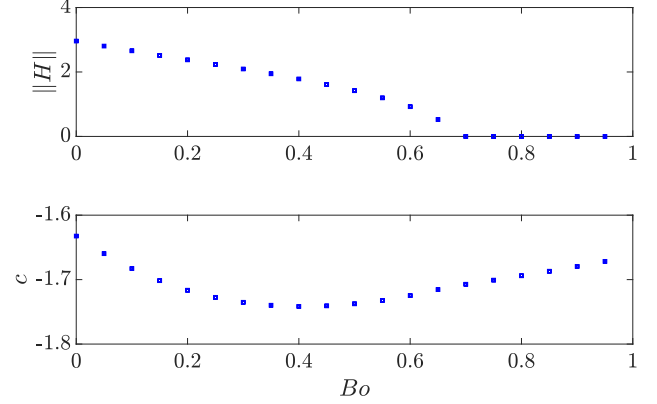

FIG. 5. Effect of the Bond number on the saturated value of the L_2-norm $\|H\|$ (or wave amplitude) and wave speed c, for the set of parameters $\nu = 0.2$, $R_e = 25$, $\Lambda = -0.25$, $A_2 = 0$, $\Gamma_0 = 1$, and $\eta = 1$.

here is to focus on the effect of density stratification on saturated solutions, therefore we will solve (28) numerically for a range of Bond numbers. The critical condition for instability can be obtained for each parametric set by fixing all of the parameters except one, and finding the value of the remaining parameter that satisfies $\Re(\sigma) = 0$ in the dispersion relation. Table I shows critical values of the Bond number Bo_c for some typical values of ν, Λ and fixed $R_e = 25$, $A_2 = 0$, $\Gamma_0 = 1$, $\eta = 1$. These values are also confirmed numerically by calculating the solution amplitude, which was found to be zero.

The influence of the Bond number on the wave amplitude and speed is demonstrated in Fig. 5, for $\nu = 0.2$, $R_e = 25$, $\Lambda = -0.25$, $A_2 = 0$, $\Gamma_0 = 1$ and $\eta = 1$. Finding the wave amplitude is mathematically equivalent to calculating the L_2-norm $\|H\|$, while the travelling-wave speed is found by setting $H(x, t) = H(x - ct)$, $\Gamma(x, t) = \Gamma(x - ct)$ in (28a) or (28b). Both of these computations are performed numerically with spectral accuracy using expressions

$$\|H\|^2 = \int_0^{2\pi} H^2 \, dx, \quad c = \lim_{t \to \infty} \frac{\int_0^{2\pi} \Gamma_x (H\Gamma)_x \, dx}{\int_0^{2\pi} \Gamma_x^2 \, dx}. \quad (29)$$

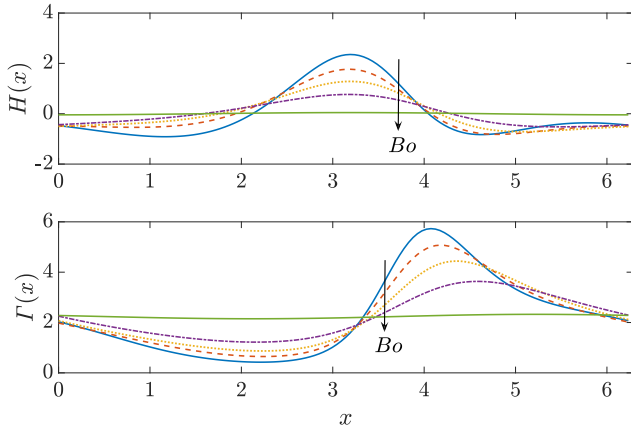The results of Fig. 5 are obtained using numerical compu-

FIG. 6. Changes in the interfacial shape $H(x)$ and surfactant concentration $\Gamma(x)$ in response to increasing the Bond number. The parameter values used are: $\nu = 0.2$, $R_e = 25$, $\Lambda = 0.25$, $A_2 = 0$, $\Gamma_0 = 1$, $\eta = 1$, and $Bo = -0.3$ (solid blue line), 0.0 (dashed orange line), 0.3 (dotted yellow line), 0.6 (dash-dotted purple line), 0.9 (solid green line). The solutions are seen to return to the trivial flat state as the Bond number increases.

tations of the unsteady problem but are also confirmed by the method of continuation (this will be described in the next section). The wave amplitude seen in the top panel of Fig. 5 diminishes when the value of the Bond number becomes greater than 0.6721, in agreement with the third column in Table I. Regardless, the wave speed illustrated in the bottom panel of Fig. 5 remains $\mathcal{O}(1)$ even after the amplitude returns to zero. The speed in the linear regime can be also found exactly by linear theory and matches the imaginary part of the growth rate. Figure 6 highlights the impact on actual saturated solutions and their shapes for $Bo = -0.3, 0.0, 0.3, 0.6, 0.9$ and $\Lambda = 0.25$ (the rest of the parameters are fixed as in Fig. 5); it is once again clear that increasing the Bond number beyond a critical value (here $Bo_c = 0.8558$ according to the fourth column of Table I) causes stabilisation of the flow.

The time evolution of the saturated interfacial and surfactant travelling waves obtained for $Bo = 0.1$ is displayed in Fig. 7. After an initial transient time, both waves are seen to preserve their shapes and travel in time with constant speed. A distinctive feature of the solutions is that they are out-of-phase, with the interfacial waves attaining a minimum around the same region where the surfactant concentration is maximised, and vice-versa. This solution characteristic is typical in problems with surfactant-laden interfaces[2–5,15] and is related to the physical mechanism responsible for the destabilisation of the interface. The mechanism can be explained by looking at the velocity perturbation at the interface $u_1(x, h(x,t), t)$, given by $\bar{u}_1(\epsilon) + m\epsilon^2 H(x,t) + \epsilon^3 \tilde{u}_1(x, h(x,t), t)$. As the highest-order velocity perturbation depends on H (through term $m\epsilon^2 H$), then at any point x^* where the interface perturbation H passes

through 0 there will be a change in the direction of the flow, with positive flow to the left and negative flow to the right of x^* (or the other way around, depending on the sign of H before and after x^* – see also Fig. 8). Therefore there will be an increase of surfactant in the vicinity of x^* as a result of the inward flow. The accumulation of surfactant around x^* then triggers the reduction of the local surface tension, which in turn gives rise to Marangoni forces that drive the fluid away from this region and towards regions of higher surface tension. This explains the interfacial minimum ahead of the surfactant-concentration maximum.

D. Bifurcation branches

The interest in this section is to determine (stable and unstable) travelling-wave solutions and their bifurcations. This can be done by the method of continuation, which employs Newton's method and follows the solutions in parameter space. Here, we use the continuation and bifurcation software AUTO-07p[26].

System (21) is considered in L-periodic domains and travelling-wave solutions are sought by writing $\zeta = x - ct$. A boundary-value problem is then solved with initial conditions chosen such that to define a bifurcation point based on linear stability theory (with a zero-amplitude amplification rate at that point) – see Appendix B for more details. We note that the calculations presented in this section are based on the localised form of system (21), obtained by utilising the approximation of $\mathcal{N}(k)$ for long waves (detailed bifurcation branches of the full nonlocal system will be reported elsewhere); in fact, it was shown by Kalogirou & Papageorgiou[5] that for relatively small Reynolds numbers (such as the value $R_e = 25$ used in this section) the nonlocal and local systems yield almost identical results.

The aim is to look for travelling-wave solution branches as the Bond number varies, therefore we perform continuation in terms of the Bond number Bo and travelling-wave speed c, while the rest of the parameters are fixed. The first set of computations uses $\nu = 0.2$, $Re = 25$, $\Lambda = -0.25$, $A_2 = 0$, $\Gamma_0 = 1$, and $\eta = 1$ and reproduces the results of Fig. 5 for Bo values that support non-trivial solutions. A second numerical calculation utilises parameters $\nu = 0.1$, $Re = 25$, $\Lambda = 0.25$, $A_2 = 0$, $\Gamma_0 = 1$, and $\eta = 1$ and the resulting bifurcation diagram is illustrated in Fig. 9. Two initial bifurcations from a flat film are seen to appear at approximately $Bo = 1.44$ and $Bo = 0.31$, respectively, confirming the results of Table I. The two bifurcation branches generated contain unimodal (branch B1, blue line) and bimodal (branch B2, green line) travelling-wave solutions, respectively – unimodal waves have wavelength equal to the whole domain length, while bimodal solutions are characterised by wavelength equal to half the length of the domain. Interestingly, the bimodal branch undergoes a bifurcation at $Bo = 0.2$ and a new branch (branch B3, orange line) hold-
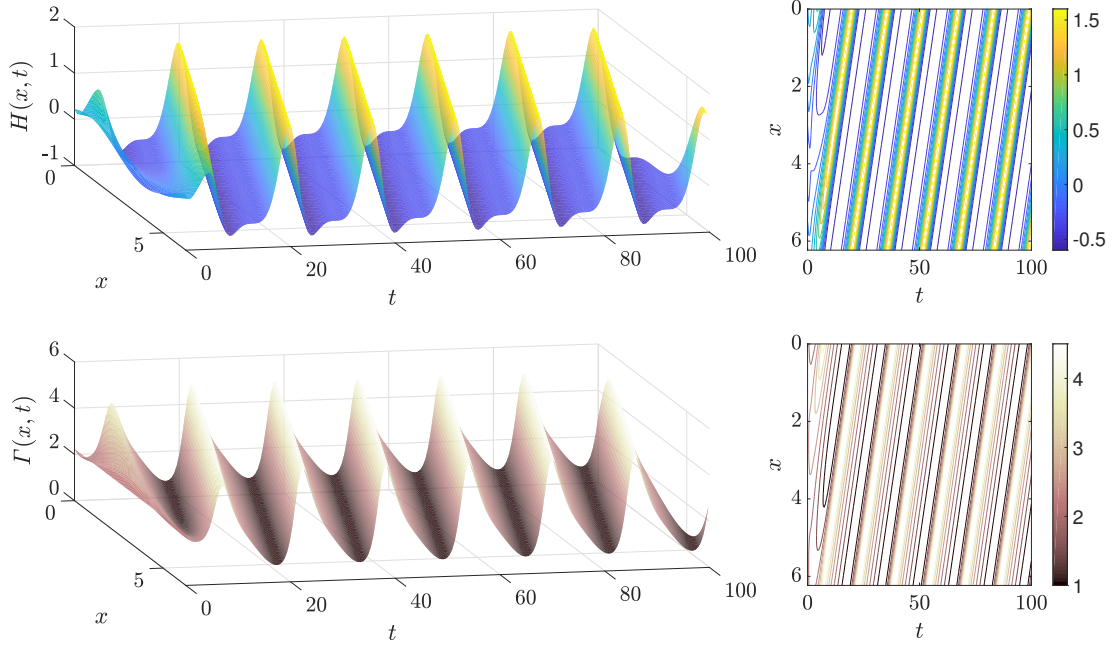
FIG. 7. Evolution of the interface perturbation $H(x,t)$ and local surfactant concentration $\Gamma(x,t)$ in time. Both solutions saturate to travelling-wave pulses after relatively short time (contour plots are depicted on the right-hand-side panels). The solutions are obtained using $\nu = 0.2$, $R_e = 25$, $\Lambda = 0.25$, $Bo = 0.1$, $A_2 = 0$, $\Gamma_0 = 1$, and $\eta = 1$.
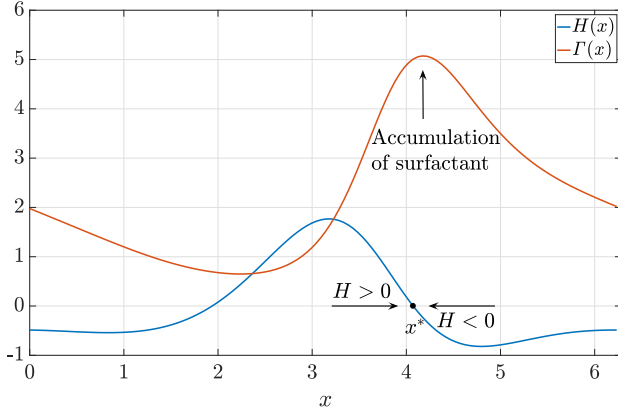

FIG. 8. Schematic explaining the mechanism responsible for destabilisation of the interface due to the presence of surfactants.

FIG. 9. Bifurcation diagram of the L_2-norm of H against the Bond number Bo, showing three branches of solutions. The rest of the parameters are set to $\nu = 0.1$, $Re = 25$, $\Lambda = 0.25$, $A_2 = 0$, $\Gamma_0 = 1$, and $\eta = 1$. The first branch B1 (blue line) corresponds to unimodal solutions, the second branch B2 (green line) to bimodal solutions, and the third branch B3 (orange line) holds unimodal solutions and is generated off the bimodal branch. The two points where the B3 branch is connected to the bimodal branch B2 are denoted with a red square.

ing unimodal higher-amplitude solutions arises. Branch B3 passes through a turning point around $Bo = -0.2$ and remerges with branch B2 at $Bo = -0.089$; the two bifurcation points connecting branches B2 and B3 are denoted with a red square in Fig. 9. Typical travelling waves obtained from the three branches are depicted in Fig. 10, where the interfacial waves $H(x)$ are displayed in the top panels and the corresponding surfactant waves $\Gamma(x)$ in the bottom panels. The three columns correspond to the
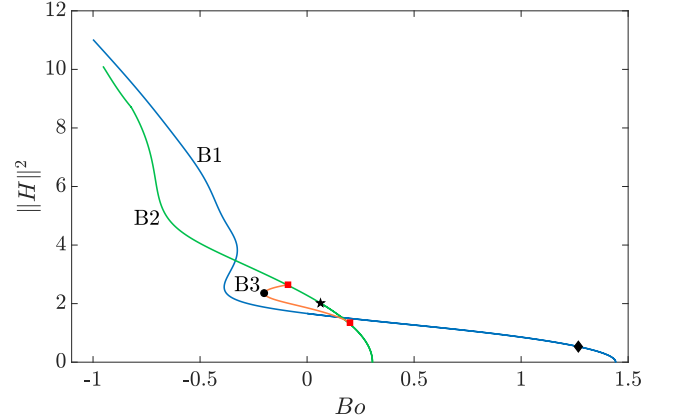
three points shown in Fig. 9 with a diamond ($Bo = 1.27$, branch B1), star ($Bo = 0.06$, branch B2), and filled circle ($Bo = -0.2$, branch B3), respectively. As the Bond num-
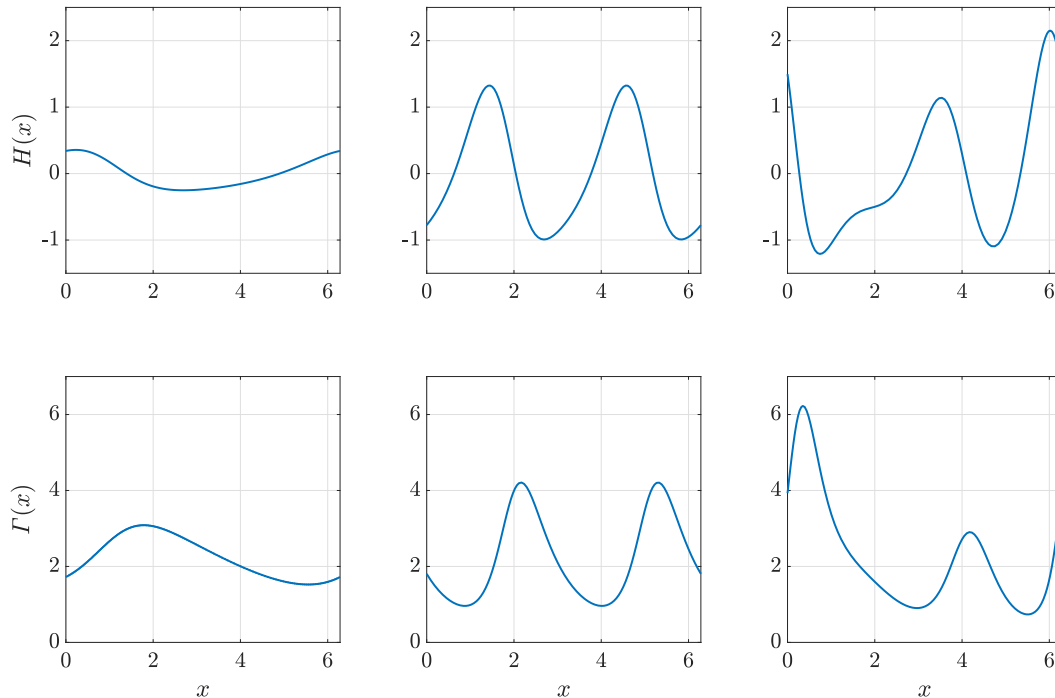
FIG. 10. Representative solutions $H(x)$ (top) and $\Gamma(x)$ (bottom) from the bifurcation diagram in Fig. 9, obtained for $Bo = 1.27$, 0.06, -0.2, respectively (moving from left to right). Each column corresponds to a set of solutions from the three branches B1, B2, and B3.

ber decreases (moving from left to right in Fig. 10) the interfacial and surfactant deflections clearly become more pronounced. Solutions in the first column already present nonlinear features that distinguish them from simple sine waves; the bimodal nature of solutions is evident in the second column, while solutions in the third column display more intricate characteristics.

We note that for $Bo = 0$ there are three solutions obtained but none of these is identical to those found in previous studies. In fact, according to Kalogirou & Papageorgiou[5] (see, for instance, their Table I), unsteady computations at $Bo = 0$ produce solutions that have the form of pulsating travelling waves, namely coherent structures with fluctuating profile and speed which are repeated after a period in time. Consequently none of the three solutions at $Bo = 0$ is stable since they do not arise as solutions of the time-dependent problem. Further stability analysis of the obtained wave branches is not performed here – this could be done following Bloch-Floquet theory[8] but is left as future work.

V. CONCLUSIONS

The stability of a surfactant-laden interface between two sheared fluids in a channel is revisited. The primary objective of this work is to investigate the interac-

tion between the various forces (Marangoni, inertial and gravitational forces) and to study the effect of gravity on the (in)stability of the interface. The problem is tackled by deriving a reduced mathematical model, valid in the limit of a thin lower fluid layer and obtained by pursuing a weakly nonlinear analysis that assumes the order of interfacial deflections to be much smaller than the thickness of the thin film. The derived model equation for the film thickness incorporates a number of competing physical forces that are relevant in thin-film flows, such as gravity (causing destabilisation of the interface when the overlying fluid is heavier), inertia in the thick fluid layer (coming into play through a nonlocal coupling term), surface tension (inducing damping of short waves), and Marangoni stresses (generated due to surfactant-concentration disturbances and resulting surface-tension gradients at the interface).

The linear stability diagram of Kalogirou & Papageorgiou[5] is extended to include the effects of stable and unstable stratification, corresponding to real situations of a lighter or heavier overlying fluid, respectively (and represented by the sign of the Bond number Bo). In the inertialess limit, a stably stratified flow can become unstable if an insoluble surfactant is present at the interface. Inertial flows are known to be unstable in the absence of surfactant (due to density and/or viscosity stratification) but stability

can be supported when a surfactant monolayer exists at the interface. The (de)stabilisation of the interface caused by the presence of surfactants can be enhanced or suppressed when gravitational forces come into play; yet, we identify regions in parameter space where the surfactant-induced instability cannot be eliminated for any value of the Bond number, however large. Additionally, the arrangement with a heavier fluid on top can be stable if the amount of surfactant, inertia and viscosity stratification are favourable, *i.e.* the values of Γ_0, R_e, Λ in our model (see stable region in Fig. 3(b)).

Nonlinear solutions of the initial-value problem arise in the form of space-periodic travelling waves, exhibiting typical features as found in related studies. The surfactant-induced mechanism responsible for the development of interfacial waves is attributed to surface-tension gradients that emerge due to non-uniform distribution of surfactant along the interface, which generate Marangoni forces that drive the fluid towards regions of high surface tension. Other forces such as inertia and gravity can also interact with the Marangoni forces and stabilise (or destabilise) the interfacial waves, which can be seen by varying the Reynolds number[5] or the Bond number, respectively.

The problem is characterised by non-uniqueness of solutions, apparent by the multiple solution branches at the same set of parameters (Fig. 9). Continuation in terms of the Bond number shows that (at least) three branches of travelling waves exist, supporting unimodal and bimodal waves. As the main goal of this work was to study the impact of density stratification on the flow, continuation on other parameters such as the Reynolds number R_e, the domain size represented through ν, and the viscosity-stratification parameter Λ has not been performed. A detailed study focusing on the various bifurcations and stability of obtained solution branches is currently under way and will be presented elsewhere.

The flow has been shown to exhibit complex spatiotemporal dynamics[4,5,15] in long channels in the absence of gravity, including a quasi-periodic route to chaos[27]. Here we have not performed simulations for increasing domain lengths, but such a study could offer a better insight into the impact of stable or unstable density stratification on these intricate dynamics. In the former case (stable density stratification), it would be interesting to investigate whether the presence of gravitational forces can delay the appearance of chaos or not. In situations with unstable density stratification, a nonlinear saturation mechanism prevents the film from rupturing[28]; yet, when gravity is strong (*i.e.* for large and negative Bo), the Rayleigh-Taylor instability becomes the predominant feature and the system is expected to eventually break down as the weakly nonlinear assumption would be no longer valid.

Appendix A: Solution in thick fluid layer

Expansions (12b) for fluid 2 are substituted into the non-dimensional momentum equations (5), yielding the steady linearised Navier-Stokes equations written below in the moving frame of reference (16)

$$\left(\bar{u}_2 - \bar{u}_1(\epsilon)\right)\frac{\partial \tilde{u}_2}{\partial \tilde{x}} + \frac{d\bar{u}_2}{dy}\tilde{v}_2 = -\frac{1}{r}\frac{\partial \tilde{p}_2}{\partial \tilde{x}} + \frac{1}{R_e}\left(\frac{\partial^2 \tilde{u}_2}{\partial \tilde{x}^2} + \frac{\partial^2 \tilde{u}_2}{\partial y^2}\right),$$
$$(A1a)$$

$$\left(\bar{u}_2 - \bar{u}_1(\epsilon)\right)\frac{\partial \tilde{v}_2}{\partial \tilde{x}} = -\frac{1}{r}\frac{\partial \tilde{p}_2}{\partial y} + \frac{1}{R_e}\left(\frac{\partial^2 \tilde{v}_2}{\partial \tilde{x}^2} + \frac{\partial^2 \tilde{v}_2}{\partial y^2}\right),$$
$$(A1b)$$

$$\frac{\partial \tilde{u}_2}{\partial \tilde{x}} + \frac{\partial \tilde{v}_2}{\partial y} = 0,\qquad (A1c)$$

with $\bar{u}_1$, $\bar{u}_2$ given in (9) and R_e the Reynolds number in the thick fluid layer. Examining the above system of equations more closely, we see that the unsteady term is missing; this is due to the slow-time transformation in (16). In addition, the term $-\bar{u}_1(\epsilon)\frac{\partial \tilde{u}_2}{\partial \tilde{x}}$ is introduced by the Galilean translation. In the problem studied here, the thin film is located near a stationary wall, thus $\bar{u}_1(\epsilon) \approx \epsilon$ and the term does not remain in (A1) at leading order.

The system (A1) is then written in Fourier space and is reduced to a fourth-order ordinary differential equation for the Fourier mode $\hat{\tilde{v}}_2(y; k)$ of wavenumber k (by eliminating the pressure $\hat{\tilde{p}}_2$ and the horizontal velocity $\hat{\tilde{u}}_2$). The no-slip condition at the upper wall and the requirement for velocity continuity at the interface provide four boundary conditions, and the solution in the upper layer can be found by solving the following Orr-Sommerfeld type boundary-value problem

$$\left(F^{(iv)} - 2k^2 F'' + k^4 F\right) - ikR_e\left(\bar{u}_2(F'' - k^2 F) + A_2 F\right) = 0,$$
$$(A2a)$$

$$F(0) = 0,\ F'(0) = 1,\ F(1) = 0,\ F'(1) = 0, \quad (A2b)$$

where $F(y)$ is connected to the vertical velocity perturbation via $\hat{\tilde{v}}_2 = -ik(m-1)\left(1 + \frac{A_2}{2}\right)\hat{H}F(y)$. Solutions of the above boundary-value problem can be obtained numerically using a finite-difference method, for instance (even though analytical expressions in terms of Airy functions can also be found[29]). Once $F(y; k)$ is known, equation (18) is readily obtained by applying inverse Fourier transform.

It is important to note that the term $-\bar{u}_1(\epsilon)\frac{\partial \tilde{u}_2}{\partial \tilde{x}}$ in (A1) should not generally be neglected, as it becomes relevant

when the interface is near a moving wall, for example if the upper fluid is thin. This case was considered in a related work by Kalogirou et al.[30], where the authors overlooked the above-mentioned term in the solution for the thick fluid. The Orr-Sommerfeld problem in that case is slightly different to (A2) as the film is located next to the moving upper wall; taking the above remarks into account, equation (3.10) in Kalogirou et al.[30] is modified by

$$\left(F^{(iv)} - 2k^2 F'' + k^4 F\right) - ikR_e(y-1)\left(F'' - k^2 F\right) = 0, \tag{A3a}$$

$$F(0) = 0, \ F'(0) = 0, \ F(1) = 0, \ F'(1) = 1. \tag{A3b}$$

It should be noted that this revised Orr-Sommerfeld problem only changes the imaginary part of the nonlocal term by decreasing it by a factor of 3, which can be incorporated in the adjustable parameter Λ in the numerical calculations. The results presented in Kalogirou et al.[30] are therefore correct but the quoted values of Λ should be 3 times bigger.

Appendix B: Implementation in AUTO-07p

The local version of system (21) in a periodic domain $[0, L]$ can be written in a system of ordinary differential equations by introducing a vector of unknowns $\boldsymbol{U} = (U_1, U_2, U_3, U_4, U_5, U_6)^T = (H, H', H'', H''', \Gamma, \Gamma')^T$ (here, prime denotes differentiation with respect to $\zeta = x - ct$), which satisfies

$$U_1' = LU_2, \tag{B1a}$$
$$U_2' = LU_3, \tag{B1b}$$
$$U_3' = LU_4, \tag{B1c}$$

$$U_4' = L\left[cU_2 - U_1 U_2 + BoU_3 \right.$$
$$\left. - \left(2\Lambda U_2 + \frac{\Lambda Re}{60}U_3 - \Lambda\left(\frac{2}{15} + \frac{Re^2}{8400}\right)U_4\right) \right.$$
$$\left. + \frac{1}{\eta}\left(-cU_6 + U_1 U_6 + U_2 U_5\right)\right], \tag{B1d}$$

$$U_5' = LU_6, \tag{B1e}$$

$$U_6' = L\left[\frac{1}{\eta}\left(-cU_6 + U_1 U_6 + U_2 U_5\right)\right]. \tag{B1f}$$

The above system has been rescaled in the domain $[0, 1]$ by introducing a scaled variable $X = \zeta/L$ and multiplying the equations by the physical domain length $L = 2\pi/\sqrt{\nu}$. The boundary-value problem is completed by introducing 4 periodic boundary conditions for variables U_1, U_2, U_3, U_5 (periodic boundary conditions for the remaining variables U_4 and U_6 are automatically satisfied in view of equations (B1)),

$$U_i(0) = U_i(1), \quad i = 1, 2, 3, 5, \tag{B2}$$

and three integral conditions fixing the mean of H to zero, the mean of Γ to Γ_0 and breaking the translational invariance of the solutions. In summary, we have a system of $N_{dim} = 6$ equations, $N_{bc} = 4$ boundary conditions and $N_{int} = 3$ integral conditions. The number of free parameters in the continuation is determined by the relation $N_{cont} = N_{bc} + N_{int} - N_{dim} + 1 = 2$, so there are two free parameters in this problem.

[1]H. A. Stone, A. D. Stroock, and A. Ajdari, "Engineering flows in small devices: microfluidics toward a Lab-on-a-Chip," Annu. Rev. Fluid Mech. **36**, 381–411 (2004).

[2]D. Halpern and A. L. Frenkel, "Nonlinear evolution, travelling waves, and secondary instability of sheared-film flows with insoluble surfactants," J. Fluid Mech. **594**, 125–156 (2008).

[3]M. G. Blyth and C. Pozrikidis, "Effect of surfactants on the stability of two-layer channel flow," J. Fluid Mech. **505**, 59–86 (2004).

[4]A. P. Bassom, M. G. Blyth, and D. T. Papageorgiou, "Nonlinear development of two-layer Couette–Poiseuille flow in the presence of surfactant," Phys. Fluids **22**, 102102 (2010).

[5]A. Kalogirou and D. T. Papageorgiou, "Nonlinear dynamics of surfactant-laden two-fluid Couette flows in the presence of inertia," J. Fluid Mech. **802**, 5–36 (2016).

[6]S. A. Kas-Danouche, D. T. Papageorgiou, and M. Siegel, "Nonlinear dynamics of core-annular film flows in the presence of surfactant," J. Fluid Mech. **626**, 415–448 (2009).

[7]A. P. Bassom, M. G. Blyth, and D. T. Papageorgiou, "Using surfactants to stabilize two-phase pipe flows of core–annular type," J. Fluid Mech. **704**, 333–359 (2012).

[8]J. Thompson and M. G. Blyth, "Inertialess multilayer film flow with surfactant: Stability and traveling waves," Phys. Rev. Fluids **1**, 063904 (2016).

[9]C.-S. Yih, "Instability due to viscosity stratification," J. Fluid Mech. **27**, 337–352 (1967).

[10]A. P. Hooper, "Long-wave instability at the interface between two viscous fluids: Thin layer effects," Phys. Fluids **28**, 1613–1618 (1985).

[11]A. L. Frenkel and D. Halpern, "Stokes-flow instability due to interfacial surfactant," Phys. Fluids **14**, L45 (2002).

[12]D. Halpern and A. L. Frenkel, "Destabilization of a creeping flow by interfacial surfactant: linear theory extended to all wavenumbers," J. Fluid Mech. **485**, 191–220 (2003).

[13]M. G. Blyth and C. Pozrikidis, "Effect of inertia on the Marangoni instability of two-layer channel flow, Part II: normal-mode analysis," J. Eng. Math. **50**, 329–341 (2004).

[14]A. L. Frenkel and D. Halpern, "Strongly nonlinear nature of interfacial-surfactant instability of Couette flow," Int. J. Pure Appl. Maths **29**, 205–223 (2006).

[15]A. Kalogirou, D. T. Papageorgiou, and Y.-S. Smyrlis, "Surfactant destabilization and non-linear phenomena in two-fluid shear flows at small Reynolds numbers," IMA J. Appl. Math. **77**, 351–360 (2012).

[16]A. L. Frenkel and D. Halpern, "Surfactant and gravity dependent instability of two-layer Couette flows and its nonlinear saturation," J. Fluid Mech. **826**, 158–204 (2017).

[17]F. Charru and E. J. Hinch, "'Phase diagram' of interfacial instabilities in a two-layer Couette flow and mechanism of the long-wave instability," J. Fluid Mech. **414**, 195–223 (2000).

[18]F. Albert and F. Charru, "Small Reynolds number instabilities in two-layer Couette flow," Eur. J. Mech. B - Fluids **19**, 229–252 (2000).

[19]H.-H. Wei, "Marangoni destabilization on a core-annular film flow due to the presence of surfactant," Phys. Fluids **17**, 027101 (2005).

[20]L. Rayleigh, "Investigation of the character of the equilibrium of an incompressible heavy fluid of variable density," Proc. London Math. Soc. **14**, 170–177 (1883).

[21] A. P. Hooper and W. G. C. Boyd, "Shear-flow instability due to a wall and a viscosity discontinuity at the interface," J. Fluid Mech. **179**, 201–225 (1987).

[22] F. Charru and J. Fabre, "Long waves at the interface between two viscous fluids," Phys. Fluids **6**, 1223–1235 (1994).

[23] G. Akrivis and M. Crouzeix, "Linearly implicit methods for nonlinear parabolic equations," Math. Comput. **73**, 613–635 (2004).

[24] G. Akrivis, D. T. Papageorgiou, and Y.-S. Smyrlis, "Linearly implicit methods for a semilinear parabolic system arising in two-phase flows," IMA J. Numer. Anal. **31**, 299–321 (2011).

[25] G. Akrivis and Y.-S. Smyrlis, "Implicit–explicit BDF methods for the Kuramoto–Sivashinsky equation," Appl. Numer. Math. **51**, 151–169 (2004).

[26] E. J. Doedel and B. E. Oldman, *AUTO-07P: Continuation and Bifurcation Software for Ordinary Differential Equations*, Concordia University (2009), available at http://cmvl.cs.concordia.ca/auto/.

[27] P. Bergé, Y. Pomeau, and C. Vidal, *Order Within Chaos: Towards a Deterministic Approach to Turbulence* (Wiley-Interscience, 1984).

[28] A. J. Babchin, A. L. Frenkel, B. G. Levich, and G. I. Sivashinsky, "Nonlinear saturation of Rayleigh–Taylor instability in thin films," Phys. Fluids **26**, 3159 (1983).

[29] A. P. Hooper and W. G. C. Boyd, "Shear-flow instability at the interface between two viscous fluids," J. Fluid Mech. **128**, 507–528 (1983).

[30] A. Kalogirou, R. Cîmpeanu, E. E. Keaveny, and D. T. Papageorgiou, "Capturing nonlinear dynamics of two-fluid Couette flows with asymptotic models," J. Fluid Mech. **806**, R1 (2016).